J Sol-Gel Sci Technol (2016) 78:613–620
DOI 10.1007/s10971-016-3999-y

ORIGINAL PAPER: SOL-GEL AND HYBRID MATERIALS FOR OPTICAL, PHOTONIC AND OPTOELECTRONIC APPLICATIONS

Demonstration of the portability of porous microstructure architecture to indium-doped ZnO electron selective layer for enhanced light scattering in inverted organic photovoltaics

Amoolya Nirmal[1] · Aung Ko Ko Kyaw[2] · Xiaowei Sun[1] · Hilmi Volkan Demir[1,3,4,5]

Received: 3 December 2015 / Accepted: 24 February 2016 / Published online: 11 March 2016

Abstract We propose and demonstrate the incorporation of porous microstructures on indium-doped zinc oxide (IZO) electron selective layer in inverted organic photovoltaics (OPV). Porosity was induced in the IZO layer with the addition of polyethylene glycol (PEG) organic template at the optimal IZO/PEG ratio of 4:1. When compared to the OPV device with non-porous IZO, the device employing porous IZO showed a 16 % improvement in current density and a 13 % improvement in efficiency. This is primarily due to the increased light scattering as substantiated by the haze factor studies. This PEG assisted method of introducing microporous structure is therefore shown to be compatible with the doped interlayer and is thus a portable method of enhancing light scattering in OPV devices.

Graphical Abstract

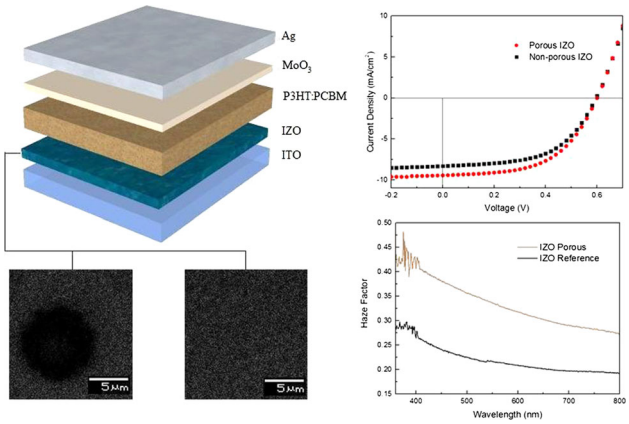

✉ Hilmi Volkan Demir
volkan@stanfordalumni.org

[1] LUMINOUS! Center of Excellence for Semiconductor Lighting and Displays, TPI- The Photonics Institute, School of Electrical and Electronic Engineering, Nanyang Technological University, Nanyang Avenue, Singapore 639798, Singapore

[2] Institute of Materials Research and Engineering, Agency for Science Technology and Research (A*STAR), Singapore 117602, Singapore

[3] School of Physical and Mathematical Sciences, Nanyang Technological University, Nanyang Avenue, Singapore 639798, Singapore

[4] Department of Electrical and Electronics Engineering, UNAM-National Nanotechnology Research Center, Bilkent University, Bilkent, Ankara 06800, Turkey

[5] Department of Physics, UNAM-National Nanotechnology Research Center, Bilkent University, Bilkent, Ankara 06800, Turkey

Keywords Indium-doped zinc oxide · Sol–gel · Porous · Organic photovoltaics

1 Introduction

The ever increasing demand for renewable energy sources to combat the ill-effects of conventional energy sources has provided impetus to the scientific research on organic photovoltaics (OPV). When compared to their inorganic counterparts, OPV provides an inexpensive route to harvest the solar energy with their inherent benefits of solution processing, ease of fabrication and compatibility with flexible substrates [1–6]. Efforts to improve the efficiency of OPV with the ultimate aim of large-scale deployment have resulted in single-cell OPV devices with an efficiency of ~9.2 % [7]. In addition to the previously reported approaches including the use of additives and mixed

solvents, novel structures, low bandgap polymers and tandem cells [8–14], the modification of metal oxide interlayers used in OPV is also an aspect that promises substantial efficiency enhancement. Metal oxide interlayers, which separate the OPV active layer from the electrodes, are an integral part of OPVs. In addition to their role as an optical spacer, metal oxide layers improve charge extraction by facilitating the transport of only one type of charge to the adjacent electrode, thus reducing recombination losses [5].

Inverted OPV architecture with the indium-doped tin oxide as a cathode and a top silver (Ag) layer as an anode is highly preferred. Inverted structures can help to overcome some of the drawbacks associated with traditional architecture, including the detrimental effect of poly(3,4-ethylenedioxythiophene)poly(styrenesulfonate)(PEDOT:PSS) interlayer on bulk hetero junction (BHJ) active layer and the use of air-sensitive aluminum as cathode layer. In inverted OPVs, n-type zinc oxide (ZnO) is used extensively as an electron transport layer due to its inherent high electron mobility and optical transparency in the visible region [15, 16]. In addition, the homogenous ZnO layer can be spin-coated from ZnO sol–gel, which is a low-cost and facile method when compared to other deposition options [17]. To improve the electrical conductivity of the ZnO sol–gel layer, various doping methods for ZnO have been previously demonstrated [18–20]. The electrons from oxygen vacancies and the zinc interstitial sites are the source of ZnO conductivity. Upon doping, substitution of the dopant ions at these interstitial sites leads to the generation of free carriers thus improving the electrical conductivity and lowering the electrical resistivity of the film. Doped ZnO films have found applications as photoconductors and sensor elements [18]. ZnO interlayers doped with aluminum [21], cesium [20] and indium [22] have been demonstrated to enhance device performance in OPVs. The increased conductivity of the doped ZnO layer also reduces internal resistance in OPV devices [20]. When compared to undoped ZnO, indium-doped ZnO (IZO) shows lower resistivity and improved transmittance without losing the aspect of solution processing [22, 23].

Nanostructured metal oxide layers with nanopillar and nanorod architectures have been widely demonstrated to enhance the OPV device performance. This is achieved by increasing the interfacial area between metal oxide and active layer, thus providing better charge collection and light trapping, and resulting in improved optical absorption [23–26]. Porous metal oxide layers have also exhibited these benefits in addition to providing an even surface topography for uniform deposition of the subsequent layers. Uneven surface topography can encourage recombination and hence result in reduction in fill factor and device efficiency [23]. ZnO porous layers have been reported to be synthesized using various methods and have found myriad applications including photocatalytic applications, antireflective coatings and gas sensing [27–32]. The use of porous ZnO structure for fabrication of hybrid OPV with ZnO and poly(3-hexylthiophene)(P3HT) has been demonstrated with substantial improvement in all device parameters [33]. We have recently studied the impact of incorporating a highly porous ZnO layer as an electron selective layer in inverted OPV and found marked improvement in efficiency when compared to inverted OPV with non-porous ZnO layer [34]. It has been suggested that ideal schemes to improve the OPV device efficiency, through enhancement of incident light absorption, should be such that they work for a broad spectrum and should be cheap and compatible with large-scale production. It should also avoid surface contamination and should not compromise the active layer quality [35]. The porous microstructure created by utilizing environmentally friendly polyethylene glycol (PEG) as a porosity-inducing organic template is a facile and inexpensive method compatible with solution processing, and if proven to be portable can be applied across a range of OPV interlayers. With this in mind, in this paper, a porous-structured indium-doped ZnO is demonstrated as an electron selective layer for poly(3-hexylthiophene) and phenyl-C61-butyric acid methyl ester (P3HT:PCBM) BHJ inverted organic solar cell. Nanopores and nanotubes with pore sizes of $\sim$10–20 nm are reported to result in polymer stacking much different from the π–π stacking of the BHJ films which has detrimental effects on device performance [36, 37]. Here, the porous IZO structure obtained by using PEG has a larger pore size and can thus ensure that the infiltrated active layer has the preferred film like properties. The porous IZO layer acts as an efficient light-scattering layer, enhancing the absorption over a broad range of spectrum, and thus improves the performance of the OPV when compared to the OPVs with non-porous IZO.

2 Experiments

The ZnO sol–gel was prepared by using the method reported in the literature [38]. Zinc acetate dihydrate was used as the precursor, and anhydrous ethanol as the solvent. The precursor was added to the solvent, and the resultant solution was refluxed for 2 h at 80 °C to form a milky solution. A stabilizing agent, monoethanolamine (MEA), was then added to obtain a clear solution, which was magnetically stirred for 12–15 h at 60 °C to obtain the ZnO sol–gel. The IZO sol–gel was obtained by adding indium chloride as a doping source to the above-mentioned ZnO sol–gel. The doping level can be precisely modulated by controlling the amount of doping source. Indium doping

was maintained at 1 at% as this doping level exhibited the best performance in previous studies [22, 39]. Lower sheet resistance and lower work function of IZO layer at this doping concentration result in better charge collection, thereby improving device performance compared to the device with undoped ZnO electron selective layer [22]. The as-prepared IZO sol–gel was used for fabrication of the non-porous IZO reference OPV device. To make porous IZO film, polyethylene glycol (PEG) was added to the as-prepared IZO sol–gel and magnetically stirred for 2 h to obtain a homogenous sol–gel before spin coating. PEG acts as a template for supporting the doped zinc oxide and also causes a phase separation between the solvent and adsorbed zinc oxide, hence facilitating the formation of the desired porous structure [17]. Upon annealing, PEG was decomposed and the porous structure was induced in the IZO layer. The degree of porosity and pore size can be varied by changing the ratio of IZO to PEG. The structures of the OPV device fabricated for the current study (ITO/IZO/P3HT:PCBM/Mo O_3/Ag) are illustrated in Fig. 1. The scanning electron microscopy (SEM) images of as-prepared samples of both porous and non-porous IZO layers are also shown in Fig. 1a, b, respectively. The micropore is clearly visible in the porous IZO layer, while the non-porous layer is featureless. For the porous and reference (non-porous) structures, the substrate, hole selective layer, active layer and silver electrode used were identical.

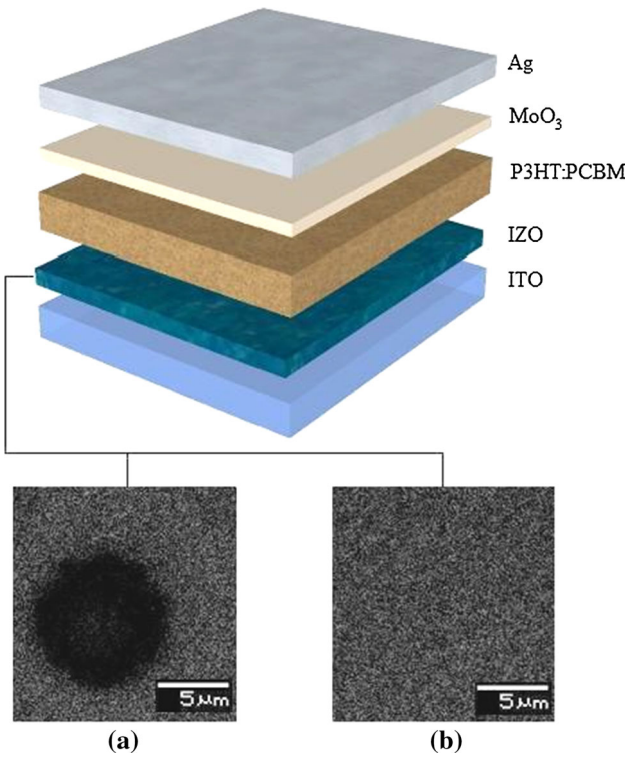

Fig. 1 Schematic representation of OPV devices fabricated along with SEM image of **a** porous IZO layer and **b** non-porous IZO layer

Indium-doped tin oxide on glass was used as the substrate. MoO_3 and silver deposited by thermal evaporation were used as the hole selective layer and electrode, respectively. A 1:1 ratio of P3HT/PCBM (40 mg/mL) in chlorobenzene solvent was used as the active layer. The difference between the structures therefore lies solely in the IZO electron selective layer employed. For the reference structure, ITO substrate was spin-coated with the as-prepared IZO sol–gel, and for the porous structure, the PEG added IZO sol–gel was spin-coated. Upon annealing, porous IZO layer was obtained for the samples coated using PEG containing IZO sol–gel due to successful removal of PEG. For optimization studies, reference samples with IZO sol–gel spin-coated at different speeds (2000, 2500 and 3000 rpm) and annealed at different temperatures (150, 200 and 250 °C) were used. Both non-porous reference samples and porous samples were then subjected to an identical processing protocol. Active layer was formed by spin coating P3HT:PCBM, with a subsequent annealing at 100 °C for 10 min. Different active layer spin-coating speeds (800–1000 and 2000 rpm) were used to study the effect of active layer spin-coating speed on the device performance. MoO_3 hole selective layer was deposited from an MoO_3 source in the molecular chamber of thermal evaporator. The pressure in the molecular chamber was kept under 10^{-4} Pa, and 15 nm of MoO_3 was deposited. Seventy nanometers of silver electrode was then deposited through a shadow mask in the metal chamber of the thermal evaporator kept under 10^{-4} Pa. The final processing step was post-anneal in N_2 ambient at 160 °C for 10 min.

The current density–voltage (J–V) characterizations for all the fabricated devices were performed under solar simulator using an AM1.5G filter calibrated to provide simulated light intensity of 100 mW/cm^2. From the J–V measurements, vital device performance parameters, such as circuit voltage (V_{oc}), short circuit current (I_{sc}), fill factor (FF) and efficiency (η), were extracted. Incident photon-to-charge conversion efficiency (IPCE) spectra were measured using a photovoltaic cell spectral response/external quantum efficiency (EQE) measurement system employing a xenon light source and triple-grating monochromator. Absorption/reflection spectra and haze factor measurements were taken with a PerkinElmer UV/Vis/NIR spectrophotometer system. The spectrophotometer provides wavelength range from 175 to 3300 nm. An integrating sphere allows for high-precision reflectance and scattered transmittance measurements.

3 Results and discussion

OPVs with indium-doped zinc oxide electron selective layers spin-coated at various speeds and annealed at a range of temperatures were analyzed. From these

optimization studies, IZO layer processed at a spin-coating speed of 2500 rpm and annealing temperature of 150 °C was found to exhibit the best performance (refer Appendix). Hence, these processing conditions were maintained for fabricating all IZO electron selective layers. Spinning speeds of active layer also had to be optimized to ensure efficient pore-filling. Inadequate pore-filling can hinder optimal device performance due to the ill-effects of thicker active layer produced at slower spinner speeds. Investigations proved that slower active layer spin speeds (800–1000 rpm) resulted in the better performance of porous IZO devices (refer Appendix). The effects of PEG concentrations on the IZO layer were also studied. The IZO/PEG ratios were varied from 2:1 to 6:1 to control the porosity and pore size by varying the PEG concentrations added to the as-prepared IZO sol–gel. For ratios below 3:1, the pronounced PEG concentration causes undesirable precipitation on the IZO layer, which reduces the wettability of the layer. The subsequent spin coating of the active layer was thus adversely affected. On the other hand, IZO/PEG ratios above 5:1 showed very low porosity and, hence, the device performance was similar to that of devices with non-porous IZO layer. Therefore, porosity studies were confined to devices with IZO layer having IZO/PEG ratios of 3:1, 4:1 and 5:1. The current density–voltage (*J*–*V*) curves of the porous and non-porous IZO devices are shown in Fig. 2. The extracted device parameters (V_{oc}, J_{sc}, FF and η) are listed in Table 1.

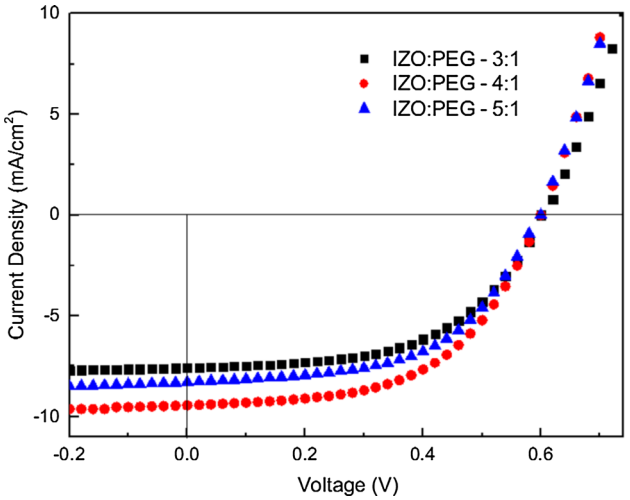

Fig. 2 Current density–voltage (*J*–*V*) characteristics of OPVs with IZO/PEG ratios of 3:1, 4:1 and 5:1

Table 1 Device parameters of OPV devices with IZO/PEG ratios of 3:1, 4:1 and 5:1

IZO/PEG ratio	V_{oc} (V)	J_{sc} (mA/cm^2)	*FF*	η (%)
3:1	0.585	−7.581	0.54	2.48
4:1	0.600	−9.436	0.54	3.07
5:1	0.601	−8.295	0.55	2.72

From Fig. 2 and Table 1, it is evident that the IZO/PEG ratio of 4:1 exhibited the optimum performance and was used to fabricate porous IZO devices for the rest of the investigations.

SEM images of the as-prepared IZO layer generated with IZO sol–gels with IZO/PEG ratios of 3:1, 4:1 and 5:1 are shown in Fig. 3. The SEM images clearly show that porosity is induced in the resultant spin-coated IZO layer by adding PEG to the IZO sol–gel. The porosity and pore size are affected by the IZO/PEG ratio. The porosity is clearly visible and the pores are well defined at the IZO/PEG ratio of 4:1.

Furthermore, the impact of porosity on device performance was evident when the best-performing porous IZO OPV device with IZO/PEG ratio of 4:1 was compared with OPV device with non-porous IZO layer. The current density–voltage (*J*–*V*) curves of the porous and non-porous IZO devices are shown in Fig. 4. The extracted device parameters are listed in Table 2.

The OPV devices with porous IZO layer was found to be as stable as the devices with non-porous ZnO layer indicting that the incorporation of porosity to the IZO electron selective layer has no noticeable detrimental effect on the stability of the OPV devices.

The properties of porous structures which lead to enhanced charge collection and light scattering improve the

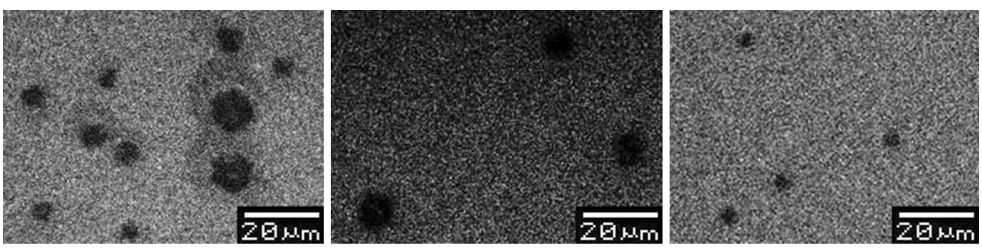

Fig. 3 SEM images of porous IZO layer with the IZO/PEG ratio of **a** 3:1, **b** 4:1 and **c** 5:1

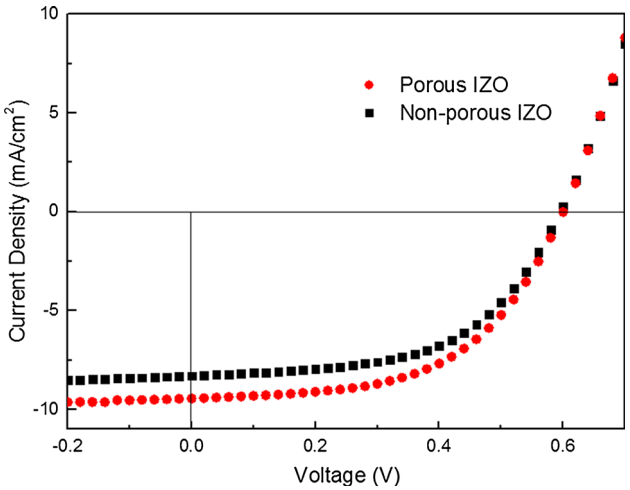

Fig. 4 Current density–voltage (J–V) characteristics of OPVs with porous and non-porous IZO electron selective layer

Table 2 Device parameters of OPV devices with porous IZO and non-porous IZO electron selective layer

	V_{oc} (V)	J_{sc} (mA/cm^2)	FF	η (%)
IZO porous	0.600	−9.436	0.54	3.07
IZO non-porous	0.603	−8.149	0.55	2.72

short circuit current density. Normalized incident photon-to-current conversion efficiency spectra of the porous and non-porous IZO electron selective layers of the devices are presented in Fig. 5. Measurements were taken on completed OPV devices. The IPCE of the porous IZO device is higher than that of the non-porous IZO device, and this is in agreement with the aforementioned short circuit current trend associated with these devices.

Absorption measurements taken on porous and non-porous IZO layers are shown in Fig. 6. Samples with the porous and non-porous IZO layers were prepared and the P3HT:PCBM BHJ active layer was spin-coated on these samples for absorption measurements. As seen in Fig. 6, porous IZO structure with IZO/PEG ratio of 4:1 shows higher absorption when compared to the sample with non-porous IZO layer. It needs to be noted that OPV devices employing ZnO nanopillars and nanorods can also lead to increased incident light absorption by the scattering provided by the nanostructures. However, the enhanced performance of such OPV devices is mainly credited to better charge collection provided by the ZnO nanopillar and nanorods [23]. These nanostructures act as antennas for the collection of dissociated electrons and provide a direct transport path to the electrode [24]. Unlike ZnO nanopillar/nanorod structures, the increased absorption exhibited by porous IZO layer can be attributed to the improved light scattering provided by the porous structure. To verify this claim, haze factor studies were carried out on the porous and non-porous samples.

A textured conductive oxide layer can scatter light effectively, and haze factor studies have been shown to quantify this scattering [40]. The total and diffuse transmittance of porous and non-porous IZO-coated ITO films were measured using PerkinElmer UV/Vis/NIR spectrophotometer system. The haze factors of the films, which are calculated as the ratio of diffuse transmittance to total transmittance, are shown in Fig. 7. Haze factor was found to be higher for the sample with IZO/PEG ratio of 4:1, indicating higher light scattering in porous samples. The porous structure thus scatters the incident light, increasing the optical path length. This efficient light scattering manifests itself as increased absorption in the BHJ active

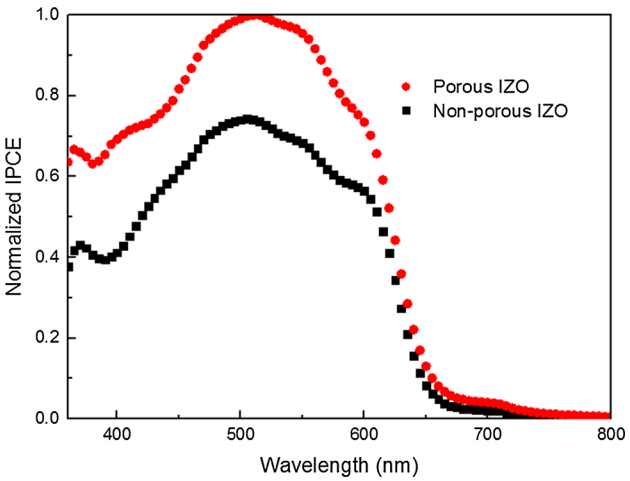

Fig. 5 Normalized IPCE spectra of OPVs with porous IZO and non-porous IZO (reference) layer

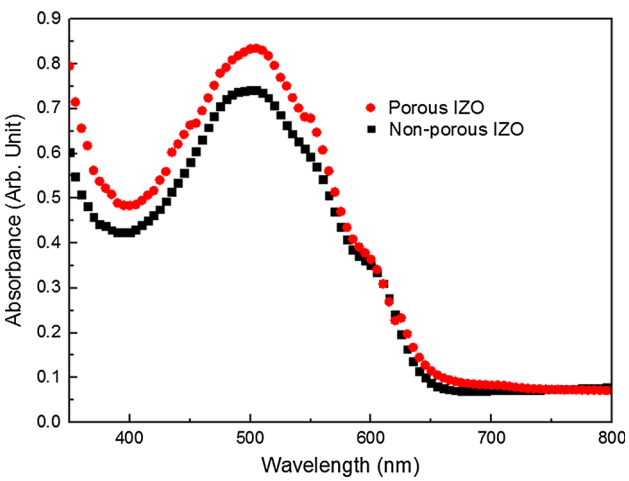

Fig. 6 Absorption spectra of OPVs with porous IZO and non-porous IZO (reference) layer

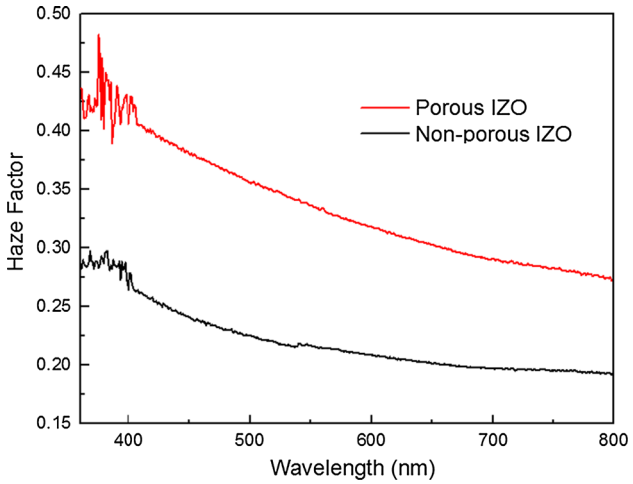

Fig. 7 Haze factor of OPVs with porous IZO and non-porous IZO (reference) layer

layer as seen in Fig. 7 thus justifying the claim of porous structure acting as efficient centers of light scattering.

The efficiency of OPV devices are heavily influenced by the type and quality of the interlayers used. The nature of the interlayer not only affects the energy level alignment, but also the active layer morphology, recombination, charge collection efficiency and device stability [15, 36, 41]. It needs to be noted that although there is an increase in the performance of OPV device with a porous IZO layer when compared to an OPV device with non-porous IZO layer, this percentage of increase is less compared to the results of a previous study involving porous ZnO layer [34]. Upon comparison of SEM images of the porous IZO and our previous report on porous ZnO, it can be observed that the porosity is higher for porous ZnO layer (refer Appendix). This higher porosity will lead to better scattering and hence higher absorption. Consequently, the enhancement in current and efficiency of OPV devices with porous ZnO is higher compared to OPV devices employing porous IZO layer. Furthermore, contact angle studies were performed using video contact analyzer to determine the wettability and adhesion properties of the porous IZO thin films. Smaller contact angles are indicative of better wettability and adhesion [42, 43]. Porous IZO had a contact angle of 68.8°. In previous studies, porous ZnO was found to have a contact angle of 59.4° [34]. The lower wettability of porous IZO indicates that the consequent spin coating of active layer will be affected. The wettability of the interlayer affects the active layer film morphology and this in turn has an impact on the absorption, charge dissociation and transport, and thus on the efficiency of the fabricated devices [15]. However, it is evident that the OPV device employing the porous IZO layer demonstrates better device efficiency when compared to its non-porous counterpart. Thus, it has been proven that, irrespective of the metal oxide interlayer used, such microporous architecture improves OPV device performance when compared to the respective non-porous interlayer thus making it a facile and portable light-scattering enhancer.

4 Conclusion

We have thus shown that increased light scattering in the porous IZO device leads to improved light trapping and hence absorption by virtue of the porous nature of the IZO electron selective layer. These OPV devices employing porous IZO exhibit improved current density and hence efficiency when compared to the reference OPV devices with non-porous IZO. Haze factor studies together with the rest of the characterization results substantiate the critical role of porous IZO as an efficient light-scattering layer in such device architectures.

Together with our previous report on OPV devices with porous ZnO, the current study also demonstrates the portability of this facile and roll-to-roll compatible method of inducing porosity using PEG in a different OPV interlayer material. Initial studies in our laboratory on using similar microporous skeletons on MoO_3 hole selective layer of standard OPV have also shown promising results, further corroborating the portability of porous microstructure architecture across different metal oxides and OPV device architectures. Hence, though the amount of efficiency improvement achieved may vary between OPV's with different metal oxide interlayers, introducing porosity in the OPV interlayer is a guaranteed method of light-scattering improvement in OPVs and can also be used in conjunction with other device performance improvement approaches.

Acknowledgments This work was supported by the Singapore National Research Foundation under Grant Nos. NRF-CRP-6-2010-2 and NRF-RF-2009-09, the Singapore Agency for Science, Technology and Research (A*STAR) SERC under Grant Nos. 092 101 0057 and 112 120 2009, the New Initiative Fund and Joint Singapore-German Research Projects from Nanyang Technological University, A*STAR SERC TSRP Grant (Grant #102 170 0137) and IMRE exploratory Project (Grant # IMRE/14-1C0247).

Appendix

OPVs with IZO electron selective layers spin-coated at various speeds and annealed at a range of temperatures were analyzed (Tables 3, 4).

From these optimization studies, IZO layer processed at spin-coating speed of 2500 rpm and annealing temperature of 150 °C was found to exhibit the best performance. Investigations proved that slower active layer spin speeds (800–1000 rpm) resulted in the better performance of porous IZO devices (Table 5).

Table 3 Device parameters of OPV devices with IZO electron selective layer at different spin speeds

IZO layer spin speed (rpm)	V_{oc} (V)	J_{sc} (mA/cm^2)	*FF*	η (%)
2000	0.581	−7.714	0.43	1.95
2500	0.595	−8.295	0.55	2.72
3000	0.606	−7.267	0.53	2.32

Table 4 Device parameters of OPV devices with IZO electron selective layer annealed at different temperatures

IZO layer anneal temperature (°C)	V_{oc} (V)	J_{sc} (mA/cm^2)	*FF*	η (%)
150	0.595	−8.295	0.55	2.72
200	0.605	−7.657	0.53	2.47
250	0.602	−7.134	0.49	2.14

Table 5 Device parameters of OPV devices with porous IZO electron selective layer with active layer spin-coated at different spin speeds

Active layer spin speed (rpm)	V_{oc} (V)	J_{sc} (mA/cm^2)	*FF*	η (%)
800–1000	0.602	−9.038	0.55	3.08
2000	0.600	−6.383	0.56	2.16

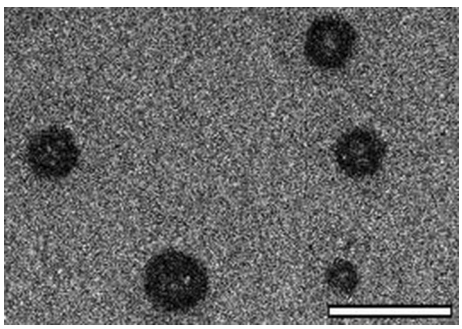

Fig. 8 SEM images of porous ZnO layer (*scale bar* is 20 μm)

SEM images of porous ZnO from our previous studies (Fig. 8) [34]. The degree of porosity for porous ZnO with ZnO/PEG ratio of 4:1 is higher when compared with porous IZO with IZO/PEG ratio of 4:1(Fig. 3b).

References

1. Jiang C, Li T, Hou L, Zhang X (2011) Research on the Characteristics of Organic Solar Cells. J Phys: Conf Ser 276(1):012169
2. Yang X, Loos J, Veenstra SC, Verhees WJH, Wienk MM, Kroon JM, Michels MAJ, Janssen RAJ (2005) Nanoscale morphology of high-performance polymer solar cells. Nano Lett 5:579–583
3. Forrest SR (2005) The limits to organic photovoltaic cell efficiency. MRS Bull 30:28–32
4. Dang MT, Wantz G, Bejbouji H, Urien M, Dautel OJ, Vignau L, Hirsch L (2011) Polymeric solar cells based on P3HT:PCBM: Role of the casting solvent. Sol Energy Mater Sol Cells 95(12):3408–3418. doi:10.1016/j.solmat.2011.07.039
5. Servaites JD, Ratner MA, Marks TJ (2011) Organic solar cells: a new look at traditional models. Energy Environ Sci 4(11):4410–4422. doi:10.1039/c1ee01663f
6. Shrotriya V, Gang L, Yan Y, Moriarty T, Emery K, Yang Y (2006) Accurate measurement and characterization of organic solar cells. Adv Funct Mater 16:2016–2023
7. He Z, Zhong C, Su S, Xu M, Wu H, Cao Y (2012) Enhanced power-conversion efficiency in polymer solar cells using an inverted device structure. Nat Photon 6 (9):591–595. http://www.nature.com/nphoton/journal/v6/n9/abs/nphoton.2012.190.html#supplementary-information
8. Yan Y, Jianhui H, Zheng X, Gang L, Yang Y (2008) Effects of solvent mixtures on the nanoscale phase separation in polymer solar cells. Adv Funct Mater 18:1783–1789
9. Sun XW, Zhao DW, Ke L, Kyaw AKK, Lo GQ, Kwong DL (2010) Inverted tandem organic solar cells with a MoO3/Ag/Al/Ca intermediate layer. Appl Phys Lett 97:053303
10. Park SH, Roy A, Beaupre S, Cho S, Coates N, Moon JS, Moses D, Leclerc M, Lee K, Heeger AJ (2009) Bulk heterojunction solar cells with internal quantum efficiency approaching 100%. Nat Photonics 3(5):297–302. doi:10.1038/nphoton.2009.69
11. Heeger AJ (2010) Semiconducting polymers: the third generation. Chem Soc Rev 39(7):2354–2371. doi:10.1039/b914956m
12. Chizu S, Yoshiaki T, Takeshi Y, Makoto K, Shuji D (2014) Recent progress of high performance polymer OLED and OPV materials for organic printed electronics. Sci Technol Adv Mater 15(3):034203
13. Lin R, Wright M, Uddin A (2013) Effects of solvent additive on inverted structure PCPDTBT: PC71BM bulk heterojunction organic solar cells. Physica Status Solidi 210(9):1785–1790. doi:10.1002/pssa.201329195
14. Ahmad R, Arora V, Srivastava R, Sapra S, Kamalasanan MN (2013) Enhanced performance of organic photovoltaic devices by incorporation of tetrapod-shaped CdSe nanocrystals in polymer–fullerene systems. Physica Status Solidi 210(4):785–790. doi:10.1002/pssa.201228347
15. Lai T-H, Tsang S-W, Manders JR, Chen S, So F (2013) Properties of interlayer for organic photovoltaics. Mater Today 16(11):424–432. doi:10.1016/j.mattod.2013.10.001
16. Chen D, Zhang C, Wei W, Wang Z, Heng T, Tang S, Han G, Zhang J, Hao Y (2015) Stability of inverted organic solar cells with low-temperature ZnO buffer layer processed from aqueous solution. Physica Status Solidi 212(10):2262–2270. doi:10.1002/pssa.201532207
17. Liu ZF, Jin ZG, Li W, Qiu JJ (2005) Preparation of ZnO porous thin films by sol-gel method using PEG template. Mater Lett 59(28):3620–3625. doi:10.1016/j.matlet.2005.06.064
18. Alam MJ, Cameron DC (2001) Preparation and properties of transparent conductive aluminum-doped zinc oxide thin films by sol-gel process. J Vac Sci Technol 19(4):1642–1646. doi:10.1116/1.1340659
19. Fathollahi V, Amini MM (2001) Sol–gel preparation of highly oriented gallium-doped zinc oxide thin films. Mater Lett 50(4):235–239. doi:10.1016/S0167-577X(01)00231-2
20. Savva A, Choulis SA (2013) Cesium-doped zinc oxide as electron selective contact in inverted organic photovoltaics. Appl Phys Lett 102(23):233301–233305
21. Murdoch GB, Hinds S, Sargent EH, Tsang SW, Mordoukhovski L, Lu ZH (2009) Aluminum doped zinc oxide for organic photovoltaics. Appl Phys Lett 94(21):213301. doi:10.1063/1.3142423

22. Kyaw AKK, Xiaowei S, De Wei Z, Swee Tiam T, Divayana Y, Demir HV (2010) Improved inverted organic solar cells with a sol–gel derived indium-doped zinc oxide buffer layer. IEEE J Sel Top Quantum Electron 16(6):1700–1706. doi:10.1109/JSTQE.2009.2039200
23. Hu ZY, Zhang JJ, Liu Y, Li YN, Zhang XD, Zhao Y (2011) Efficiency enhancement of inverted organic photovoltaic devices with ZnO nanopillars fabricated on FTO glass substrates. Synth Met 161(19–20):2174–2178. doi:10.1016/j.synthmet.2011.08.025
24. Ju XH, Feng W, Varutt KC, Hori TS, Fujii AH, Ozaki MN (2008) Fabrication of oriented ZnO nanopillar self-assemblies and their application for photovoltaic devices. Nanotechnology. doi:10.1088/0957-4484/19/43/435706
25. Olson DC, Yun-Ju L, White MS, Kopidakis N, Shaheen SE, Ginley DS, Voigt JA, Hsu JWP (2007) Effect of polymer processing on the performance of poly(3-hexylthiophene)/ZnO nanorod photovoltaic devices. J Phys Chem C 111:16640–16645
26. Takanezawa K, Hirota K, Wei QS, Tajima K, Hashimoto K (2007) Efficient charge collection with ZnO nanorod array in hybrid photovoltaic devices. J Phys Chem C 111(19):7218–7223. doi:10.1021/jp071418n
27. Zhifeng L, Zhengguo J, Jijun Q, Xiaoxin L, Weibing W, Wei L (2006) Preparation and characteristics of ordered porous ZnO films by a electrodeposition method using PS array templates. Semicond Sci Technol 21(1):60
28. Liu Z, Jin Z, Li W, Qiu J, Zhao J, Liu X (2006) Synthesis of PS colloidal crystal templates and ordered ZnO porous thin films by dip-drawing method. Appl Surf Sci 252(14):5002–5009. doi:10.1016/j.apsusc.2005.07.018
29. Wang L, Zheng Y, Li X, Dong W, Tang W, Chen B, Li C, Li X, Zhang T, Xu W (2011) Nanostructured porous ZnO film with enhanced photocatalytic activity. Thin Solid Films 519(16):5673–5678. doi:10.1016/j.tsf.2011.02.070
30. Rakibuddin M, Ananthakrishnan R (2016) Novel nano coordination polymer based synthesis of porous ZnO hexagonal nanodisk for higher gas sorption and photocatalytic activities. Appl Surf Sci 362:265–273. doi:10.1016/j.apsusc.2015.11.206
31. Li D, Huang F, Ding S (2011) Sol–gel preparation and characterization of nanoporous ZnO/SiO2 coatings with broadband antireflection properties. Appl Surf Sci 257(23):9752–9756. doi:10.1016/j.apsusc.2011.05.126
32. Zhu Y, Wang Y, Duan G, Zhang H, Li Y, Liu G, Xu L, Cai W (2015) In situ growth of porous ZnO nanosheet-built network film as high-performance gas sensor. Sens Actuators B Chem 221:350–356. doi:10.1016/j.snb.2015.06.115
33. Boucle J, Snaith HJ, Greenham NC (2010) Simple approach to hybrid polymer/porous metal oxide solar cells from solution-processed ZnO nanocrystals. J Phys Chem C 114(8):3664–3674. doi:10.1021/jp909376f
34. Nirmal A, Kyaw AKK, Sun XW, Demir HV (2014) Microstructured porous ZnO thin film for increased light scattering and improved efficiency in inverted organic photovoltaics. Opt Express 22(S6):A1412–A1421. doi:10.1364/OE.22.0A1412
35. Cho C, Kim H, Jeong S, Baek S-W, Seo J-W, Han D, Kim K, Park Y, Yoo S, Lee J-Y (2013) Random and V-groove texturing for efficient light trapping in organic photovoltaic cells. Sol Energy Mater Sol Cells 115:36–41. doi:10.1016/j.solmat.2013.03.014
36. Chen L-M, Xu Z, Hong Z, Yang Y (2010) Interface investigation and engineering - achieving high performance polymer photovoltaic devices. J Mater Chem 20(13):2575–2598. doi:10.1039/B925382C
37. Mor GK, Shankar K, Paulose M, Varghese OK, Grimes CA (2007) High efficiency double heterojunction polymer photovoltaic cells using highly ordered TiO2 nanotube arrays. Appl Phys Lett 91(15):152111. doi:10.1063/1.2799257
38. Kyaw AKK, Sun XW, Jiang CY, Lo GQ, Zhao DW, Kwong DL (2008) An inverted organic solar cell employing a sol-gel derived ZnO electron selective layer and thermal evaporated MoO3 hole selective layer. Appl Phys Lett 93(22):221107. doi:10.1063/1.3039076
39. Kyaw AKK, Wang Y, Zhao DW, Huang ZH, Zeng XT, Sun XW (2011) The properties of sol–gel processed indium-doped zinc oxide semiconductor film and its application in organic solar cells. Physica Status Solidi 208(11):2635–2642. doi:10.1002/pssa.201127263
40. Hsiao YS, Chen CP, Chao CH, Whang WT (2009) All-solution-processed inverted polymer solar cells on granular surface-nickelized polyimide. Org Electron 10(4):551–561. doi:10.1016/j.orgel.2009.01.012
41. Steim R, Kogler FR, Brabec CJ (2010) Interface materials for organic solar cells. J Mater Chem 20(13):2499–2512. doi:10.1039/B921624C
42. Dupont SR, Voroshazi E, Heremans P, Dauskardt RH (2013) Adhesion properties of inverted polymer solarcells: processing and film structure parameters. Org Electron 14(5):1262–1270. doi:10.1016/j.orgel.2013.02.022
43. Kyaw AKK, Sun XW, Jiang CY, Lo GQ, Zhao DW, Kwong DL (2008) An inverted organic solar cell employing a sol-gel derived ZnO electron selective layer and thermal evaporated MoO3 hole selective layer. Appl Phys Lett 93:221107